High frequency valve development for smart material electro-hydraulic actuators

John P. Larson and Marcelo J. Dapino

Smart Vehicle Concepts Center, Department of Mechanical & Aerospace Engineering
The Ohio State University, Columbus, OH, 43210

ABSTRACT

This paper presents two approaches to developing improved check valves for high frequency fluid rectification in a smart material electro-hydraulic actuator: a single reed-type design and an array of miniaturized valves. The multiphysics software COMSOL was used to study the 3-D fluid-structure interaction between the valve and hydraulic fluid during pump operation, and the results were validated utilizing an instrumented valve to measure in-situ tip displacement. The added mass effect of the fluid on the valve was experimentally characterized. To improve the frequency response of the valves, an array of miniature reed valves were designed for the high frequency and high pressure environment in the pump. A fabrication method was developed for the miniaturized valves utilizing micromachining processes. The performance of the two types of valves was compared through static and dynamic experiments.

Keywords: Terfenol-D, magnetostrictive pump, reed valves, hydraulic rectification, electro-hydraulic actuator

1. INTRODUCTION

Smart material electro-hydraulic actuators take advantage of the high force and fast frequency response of smart materials such as piezoelectrics and magnetostrictives. Hydraulic rectification is used to create large displacements from the relatively small, high-frequency displacements of a smart material pump. The rectification of fluid pulses is done with check valves. Electro-hydrostatic actuators are attractive as a potential replacement to hydraulic pistons in aerospace and automotive applications where size and weight are of concern.

Designing check valves to perform the fluid rectification at frequencies above 1 kHz has proven difficult. An array of miniature valves can increase the frequency response of check valves by decreasing the size and mass of each valve while maintaining the overall valve stiffness and flow rate. Previous attempts to develop miniature valve arrays for hydraulic actuators include silicon valves developed by Lee et al.[1] and nickel valves made by Li and Chen.[2] Both of these valve designs were manufactured using chemical etching processes and photolithography to selectively remove material from the substrate to make the different valve layers. As reported by O'Neill and Burchfield,[3] the silicon valves failed when tested at pump pressures and the nickel valves produced unacceptably high back flows because of fabrication defects (residual material from the fabrication process). Seong et al.[4] also used Nitinol to design a valve array taking advantage of the high strains (up to 10%) available due to the pseudoelastic effect. However, testing was limited to static flow conditions; fatigue life considerations may limit the available strains for high frequency pump applications.[5]

Larger one-way valves consisting of a single thin metal reed covering an inlet hole have been studied for smart material electro-hydraulic style pumps. Chaudhuri et al.[6] considered the coupling between fluid flow and valve displacement in a 2-D finite element analysis of reed valves. Walters[7] presented flow resistance calculations based on 3-D CFD model which considers a static reed geometry.

This paper studies both types of valves. A detailed 3-D CFD model is used to analyze the flow though a single-reed valve, and these results are validated with testing on larger, conventional reeds. A design for a miniaturized reed valve array is presented along with static and dynamic testing results.

Further author information: (Send correspondence to M.J.D.)
M.J.D.: E-mail: dapino.1@osu.edu, Telephone: 1-614-688-3689
J.P.L.: E-mail: larson.303@osu.edu, Telephone: 1-614-247-7480

Industrial and Commercial Applications of Smart Structures Technologies 2011,
Edited by Kevin M. Farinholt, Steve F. Griffin, Proc. of SPIE Vol. 7979, 79790E
 · doi: 10.1117/12.881958

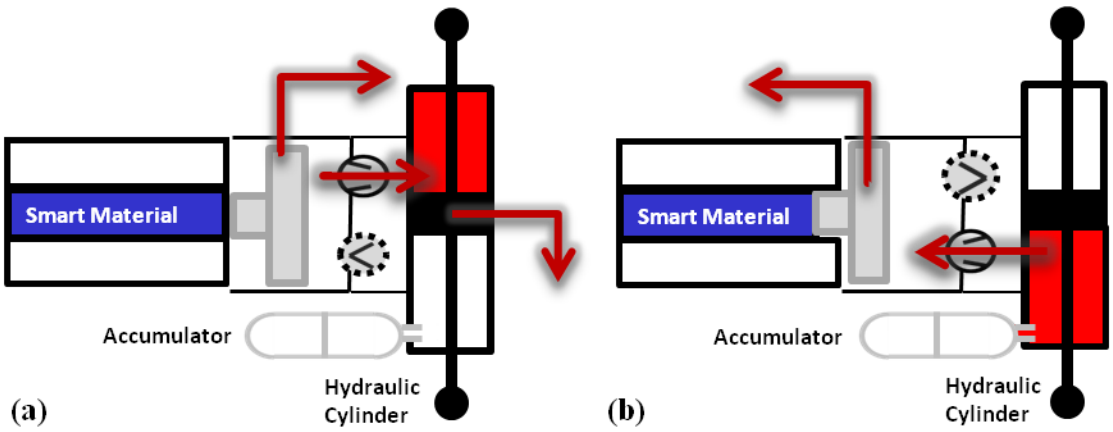

Figure 1. Electro-hydraulic actuator principle of operation, showing the flow of fluid corresponding to the compression (a) and return (b) strokes of the smart material driver.

2. PUMP PRINCIPLE OF OPERATION

The principle of operation for a smart material electro-hydraulic actuator is shown in Fig. 1. The pump is driven by a smart material rod, which could be either piezoelectric or magnetostrictive. A signal, typically sinusoidal, is applied to the smart material driver, causing the rod to alternatively extend and contract. The extension part of the stroke compresses hydraulic fluid in the pump chamber. Check valves direct the fluid flow causing fluid at high pressure to flow into a hydraulic cylinder, causing it to move. As the piston retracts for the second half of the stroke, the outlet check valve closes, holding the high-side hydraulic cylinder pressure. The inlet check valve then opens to draw in fluid from the low-pressure side of the hydraulic cylinder into the pumping chamber to refill it for the next compression stroke. An accumulator on the low pressure side of the hydraulic cylinder maintains a bias pressure to keep the smart material driver in compression and prevent cavitation.

With appropriate valving, the concept could be used for bi-directional operation of the hydraulic cylinder. However, for simplicity the tested pump was configured to actuate in one direction. A manual return valve was used to reset the cylinder between runs.

3. CFD ANALYSIS

The multiphysics software COMSOL was used to study the 3-D fluid-structure interaction between the valve and hydraulic fluid during pump operation. The single-reed valve and pump valve port geometry was chosen for analysis to facilitate validation experiments. Figure 2 shows the 3-D geometry of the reed valves and fluid passage used for finite element analysis. The deformation of the valve due to fluid pressure and the flow around the deformed valve geometry were solved simultaneously.

Figure 2 shows the geometry for modeling the reed valve flow. A constant pressure differential was applied between the inlet and outlet, and the resulting flow rate and valve displacement were calculated. A fixed boundary condition was applied at the base of the valve, and a no-slip condition was applied to the walls.

To keep the fluid domain continuous, an offset is needed between the valve and valve seat in the initial geometry. This offset was kept small to minimize its effect on the solution. An arbitrary Lagrangian-Eulerian (ALE) finite element formulation was used to deform the mesh and track the motion of the valve with applied pressure. Several levels of mesh refinement were used to improve the correlation of the model results with experimental data. An issue that arises as the size of the mesh elements decreases is that with the initial model, the mesh deformation in the fluid region is confined to only the elements nearest the valve. To improve the quality of the mesh, several prescribed displacement surfaces were added between the valve and the valve seat to evenly distribute the deformation (Fig. 3).

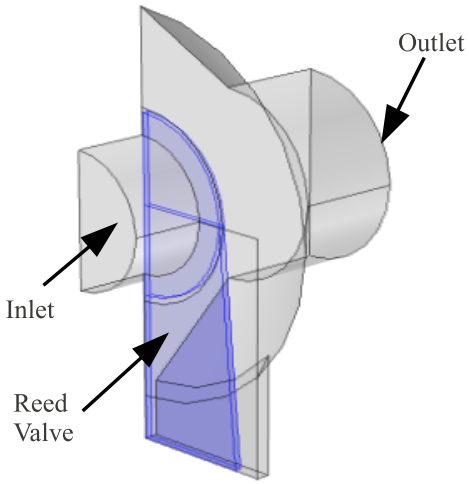

Figure 2. 3-D geometry used for COMSOL Multiphysics modeling of the conventional reed valve.

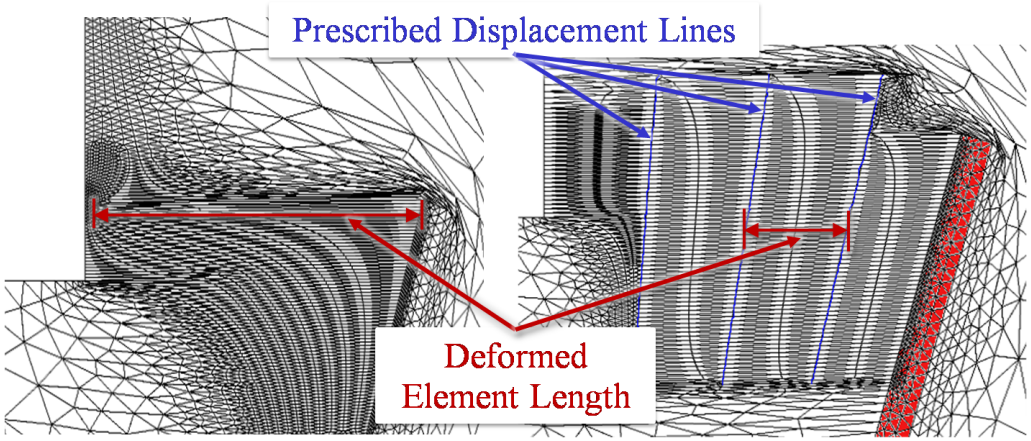

Figure 3. Two-dimensional representation of the reed valve solution geometry demonstrating improvement in element quality using a prescribed mesh displacement. (Deformations are exaggerated for illustration.)

4. VALVE DESIGN

An array of 21 miniature reed valves was developed for testing within an existing electro-hydrostatic actuator (Fig. 4). Stainless steel was chosen as the valve material due to its corrosion resistance and well-known fatigue behavior. The valve design consists of four layers: inlet, valve, spacer, and outlet. The valve layer contains the valve flaps, which cover holes in the inlet layer. The outlet layer contains both the fluid flow path and stops to limit the travel of the valves. The maximum distance that the valves could open is determined by the thickness of a spacer layer between the valve layer and the outlet layer. The overall size of the valve array was limited to a diameter of 6.4 mm (0.25 in) by the valve port in the pump.

Design for infinite fatigue life was considered for the high-frequency, high-pressure environment in the pump. An allowable stress of 390 MPa (56 ksi) was calculated for the 301 fully hardened stainless steel used in the design.[8,9] Two extreme cases were considered for the analysis: full valve displacement and blocked pump pressure. The displacement is limited by the designed thickness of the spacer layer (25 μm), and the maximum blocked pressure capability of the pump was determined in previous experiments to be approximately 10 MPa (1500 psi). ANSYS was used to analyze the stress in each of these cases and the design was iterated to reduce the stress below allowable levels. The maximum stress was calculated to be 360 MPa for the fully open valve

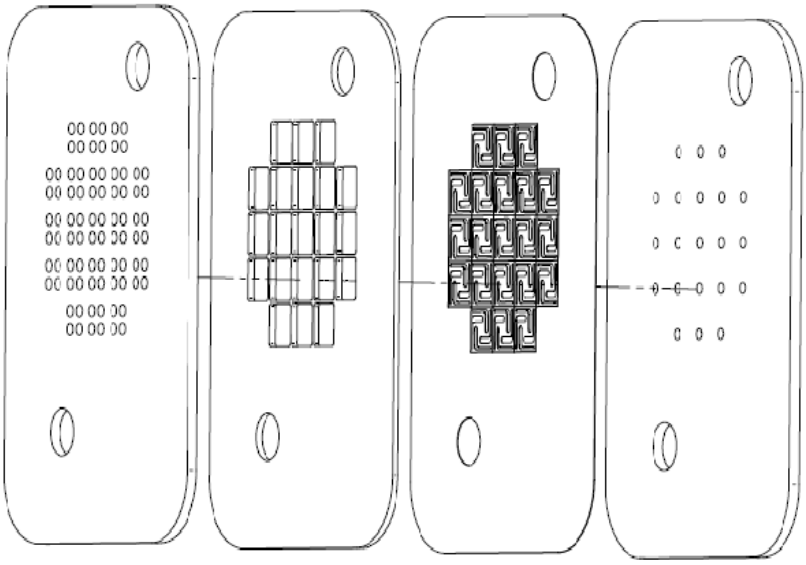

Figure 4. Design of the miniature reed valve array layers: outlet layer, spacer layer, valve layer, and inlet layer (left to right). Two large holes are provided on each part for alignment pins.

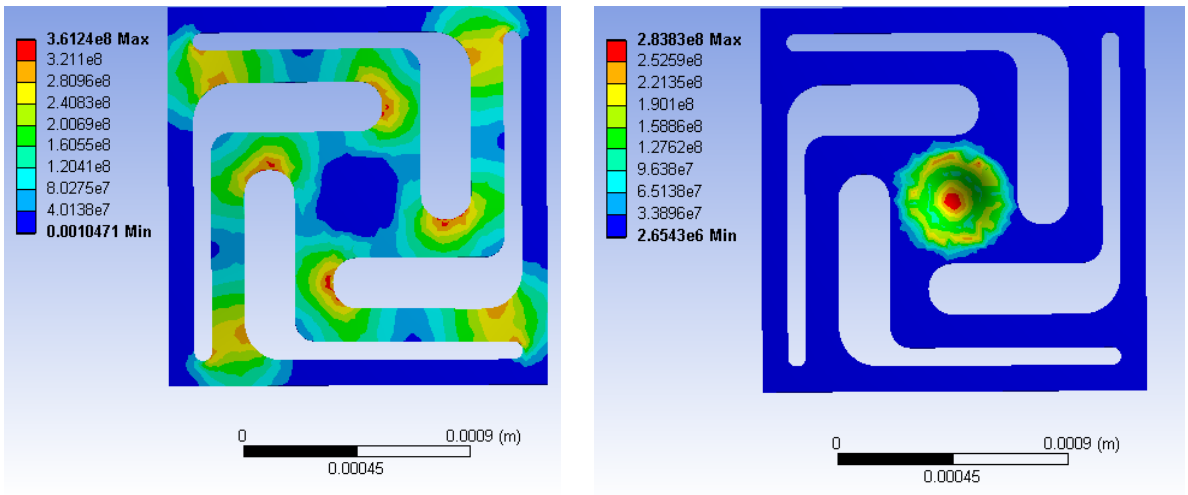

Figure 5. Stress distribution calculated with ANSYS of the miniature reed at maximum valve opening of 25 μm (left) and at zero opening with maximum pump blocked pressure of 10 MPa (right).

and 280 MPa for the maximum pump pressure level (Fig. 5).

As designed, the reed valves consist of 500 μm square flaps with four spring arms (Fig. 6). These flaps each cover a 360 μm diameter hole in the inlet valve layer, which is 700 μm thick. The maximum stress on the inlet layer with a 10 MPa blocked pressure was calculated to be 300 MPa, within acceptable levels. The outlet layer is 300 μm thick.

For adequate operation in the EHA pump at frequencies over 1 kHz, it is desired for the valve natural frequency to be well above this value. The first natural frequency of the valve design was calculated as 20.7 kHz using ANSYS. The design of the four valve layers is shown in Fig. 4; alignment holes are provided to keep the different layers aligned with pins. The valve and spacer layers were laser cut from 25 μm thick stock. The thicker inlet and outlet layers were fabricated with micromachining processes.

The performance of the miniature valve array was compared to the existing single reed valves.[10] These valves

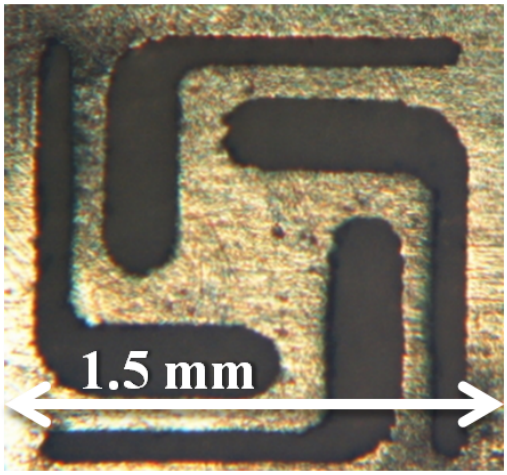

Figure 6. Close up of a single miniature reed valve.

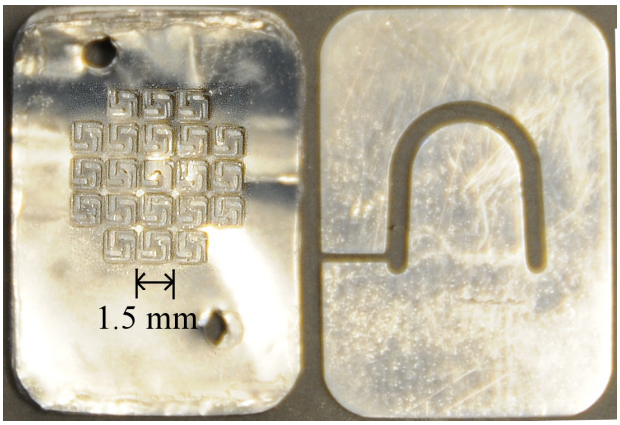

Figure 7. Miniature reed valve array (left) and conventional reed valve (right).

are made from 0.127 mm (0.005") thick stainless steel (Fig. 7). To calculate the frequency response of the single-reed valves, the curved geometry of the valve was approximated by a 7 mm x 5 mm rectangular plate.[11] The effect of the added mass of the hydraulic fluid was calculated as described in the appendix.

The relationship between volumetric flow Q and pressure differential ΔP for both sets of valves can be described by the general form of the orifice flow equations

$$\Delta P = \frac{\rho}{2} \frac{1}{(C_d A_0)^n} Q^n, \tag{1}$$

where A_0 is the flow area, C_d and n are flow coefficients.[12] For a sharp-edged orifice, these coefficients are typically assumed to be $C_d = 0.61$ and $n = 2$, but they may need to be experimentally determined for the complex geometries in the valves. The flow can also be described as a hydraulic resistance $R = \frac{\Delta P}{Q}$, which is a function of the valve displacement.

5. EXPERIMENTAL METHODS

The valves were tested statically to determine their flow resistance characteristics, and their performance in the smart material actuator was established. To create conditions matching the CFD results, a valve holder was created to match the inlet and outlet channels and the valve port geometry of the pump. A fluid reservoir supplied Mobil DTE 24 hydraulic fluid at a constant pressure maintained by a compressed nitrogen cylinder and regulator. The mass flow rate of the fluid was measured with a scale and the pressure differential across the valve was measured using two Sensotec 7351-02 pressure sensors. These tests were conducted on both the miniature valve array and the single-reed valves over a range of pressures. The inlet and outlet layers of the miniature valve array were tested separately to measure their effects on the flow as well.

An additional test measurement of the valve displacement was taken for the single-reed valves. These valves were large enough that a strain gage could be affixed to the valve base. The amount of strain was measured during the flow tests, and this was correlated to the valve displacement with a separate experiment comparing the strain to displacements measured with a laser displacement sensor.

To better assess the dynamic response of the single-reed valves, these valves were tested to determine their frequency response characteristics. The valves were clamped in a test holder, and then manually displaced a small amount. This displacement was then released, and the valve oscillations returning back to zero displacement were measured using both a non-contact laser displacement sensor and a strain gage. The damped natural frequency of oscillation was measured and the damping ratio was calculated from the log decrement. Comparison of the test results before and after adding the strain gage to the valve demonstrates that the strain gage had a negligible

effect on the valve response. The valve was then tested submerged in hydraulic fluid to determine the added mass and damping of the fluid. Strain measurements were used to determine the damped natural frequency and damping. The results were compared to analytic predictions of the valve response.

Each set of valves was then tested in the pump to determine their effect on overall pump performance. A constant sinusoidal current of 3.5 A_{rms} was applied at each frequency for all tests. A bias pressure of 2.6 MPa (375 psi) was used for testing, resulting in a pre-load of 10.3 MPa (1.5 ksi) on the Terfenol-D driver. Further testing on the pump included a blocked pressure sweep. A lower sinusoidal current of 1.4 A_{rms} was applied over a broader frequency range and the blocked pressure generated by the pump was measured at each frequency. For comparison, the same test was also conducted without valves installed, measuring the amplitude of the pressure wave generated.

6. RESULTS AND DISCUSSION

Using the COMSOL fluid-structure interaction model, the flow resistance of the single-reed valve was calculated as a function of tip displacement (Fig. 8). The results demonstrate a fairly good correlation with experimental data from static testing on the instrumented valve. The use of two prescribed mesh displacement surfaces improved the results by distributing the mesh deformation to track the valve motion evenly across the mesh elements.

Dynamic test results for the single-reed valve are summarized in Table 1. The effect of adding the strain gage to the valve was found to be small; there is only a 3% variation in the measured natural frequency in air. This difference could be attributed to a slight variation (less than 0.1 mm) in the clamped length of the valve between tests. The results demonstrate that the added mass factor from (3) accounts for the effect of the fluid on the reed valve dynamic response. The damping ratio was calculated using the log decrement of the response as 0.0036 for the reed in air and 0.076 for the reed in fluid.

Figure 9 shows the results of static testing on the miniature valve array. The valves were tested for both forward and reverse (leakage) flow. A small amount of back flow (approximately 0.5 cm^3/s) was measured over the full range of pressures tested (0 - 1.4 MPa). This back flow is likely a result of oxidation remaining from the laser cutting process. A polishing step was used to remove much of the oxidation but not all, which may have lowered the sealing ability of the valves (Fig. 10).

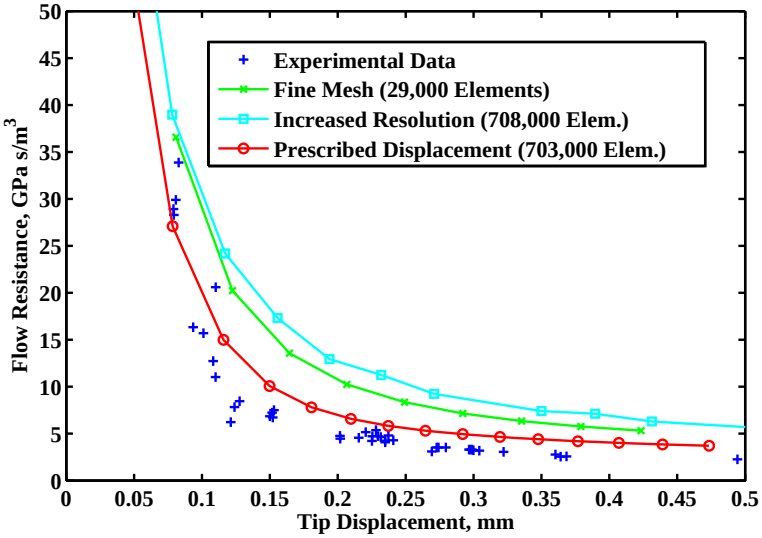

Figure 8. Reed valve flow resistance compared to tip displacement comparing experimental results with COMSOL calculations. The default "fine" mesh is compared with a higher mesh resolution, with and without the prescribed mesh displacement surfaces.

Table 1. Results of reed natural frequency testing comparing the analytical calculations of the damped natural frequency of the reeds in air and hydraulic fluid with measured values.

	f_1 (Air)	f_1 (Fluid)
Calculated	2155	1190
Laser Sensor Only	2100	N/A
Strain Gage & Laser	2160	1170

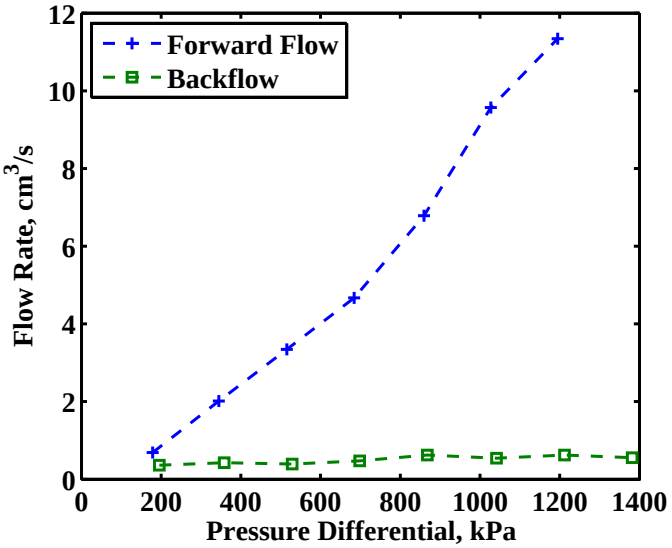

Figure 9. Measured flow rate vs. differential input pressure measured for the miniature reed array. The pressure was applied in the forward (valve opening) and reverse (valve leakage) directions.

Figure 11 compares the static test results from the miniature reed valve array to the single-reed valve. The miniature reed valve array exhibits a significantly higher resistance to flow than the single-reeds with an applied pressure of 1200 kPa required to achieve 12 cm^3/s flow compared to 47 kPa for the single-reed. This increase in flow resistance was expected because the miniature reed valve array design was constrained to fit within the existing valve port used by the single-reed valve, limiting the available flow area.

The miniature reed valve design successfully rectified flow and withstood high pressure pump operation (Fig. 12). A peak unloaded velocity of 33 mm/s was measured at a pumping frequency of 200 Hz. The performance leveled off at higher frequencies with 29 mm/s measured at 650 Hz. This velocity was lower than the peak velocity of 74 mm/s achieved at 300 Hz using single-reed valves, as expected due to the higher flow resistance of the miniature reed array.

The blocked pressure, which is the amount of pressure that the pump generates with the actuator fixed, depends less on the flow area since the pump can build up pressure over many cycles. To compare the two types of valves, this pressure was measured up to 1300 Hz for a constant sinusoidal current applied (Fig. 13). The resulting blocked pressure for the miniature reeds is approximately two-thirds of the single-reed result for a large portion of the test. This decrease can attributed to the back flow noted in the miniature reeds during the static tests. The results are worse at low frequencies, where there is more time for the pressure to bleed off between pump cycles. It is emphasized that the blocked pressure for both types of valves decreases rapidly at frequencies above 1000 Hz, indicating that a common factor may be attenuating the pressure at high frequencies. To isolate the effect of the pump and manifold from the valves, the same frequency sweep was performed without the valves installed, measuring the magnitude of the pressure output instead of the blocked pressure. There is one peak at 1825 Hz, which can be attributed to the transducer resonance.[13] The results below 1000 Hz show a double-peaked response, at frequencies similar to the peaks in the unloaded actuator velocity tests. After the second peak, there is a sharp decrease in the measurement which matches the reduction in response of the valves

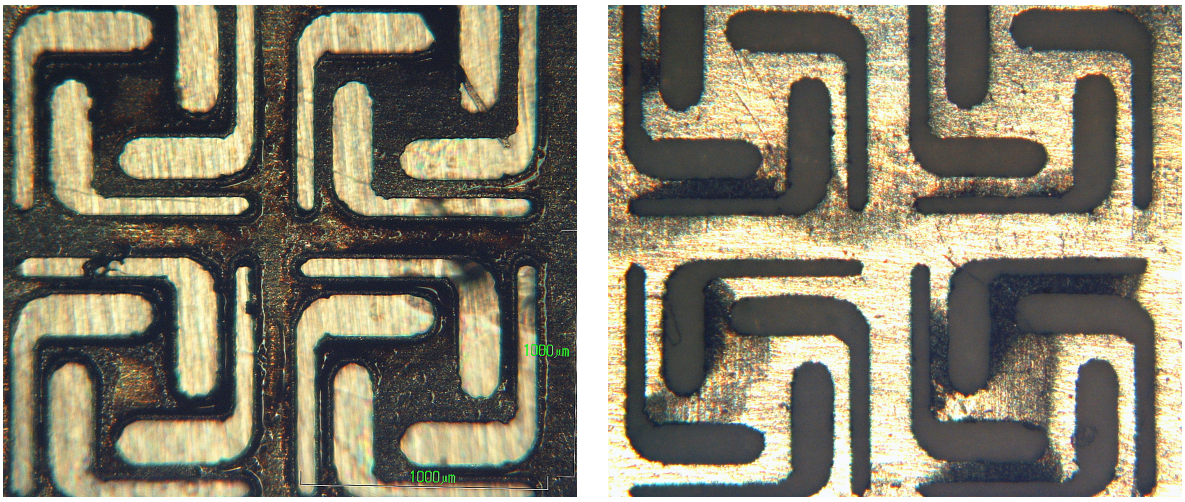

Figure 10. The as-received condition of the miniature reeds had a large amount of oxidation remaining from the laser cutting process (left). A polishing step removed much of this oxidation but a some amount remained (right).

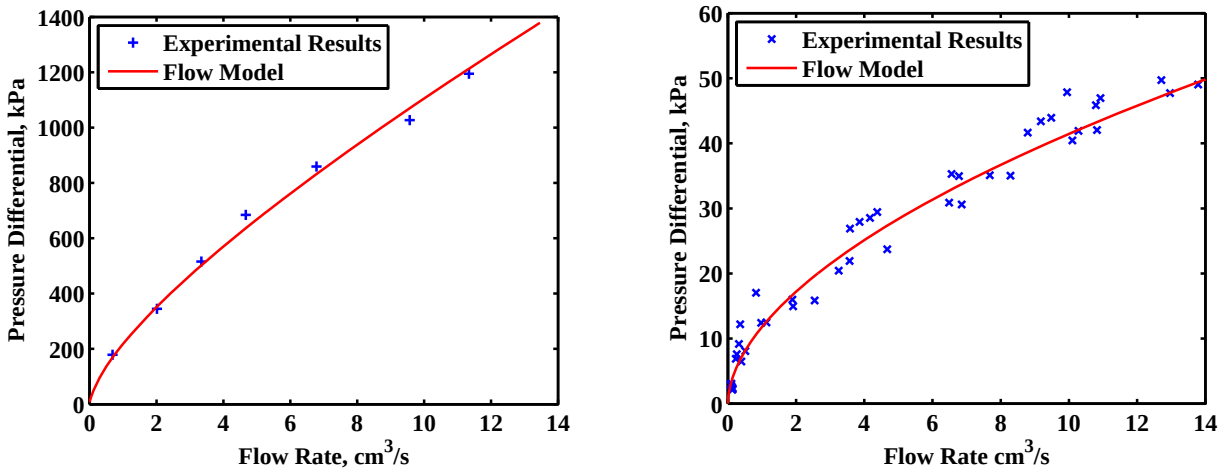

Figure 11. Comparison of static tests results measuring the flow rate vs. the applied pressure differential for the miniature reed valve array (left) and the single-reed valve (right). Model results using (1), and assuming $C_d = 0.61$ and $n = 2$ for the miniature reeds and $C_d = 0.21$ and $n = 1.35$ for the single-reed are shown in red.

from the blocked pressure test. This indicates that the manifold and pump, rather than the valves, may have been limiting the overall actuator bandwidth.

7. CONCLUSIONS

This paper demonstrated that the novel design for miniature reed valves, with each layer machined separately using micromachining processes, successfully rectified fluid flow. The design was proven to be robust, successfully surviving the high-pressure and high frequency operation of the pump. The measured flow rates from the miniature reed valves are lower than the flow rates for the single-reed valves, but this is expected because the mini-reed array design utilizes the existing valve ports at a penalty of greatly reduced available flow area. Experimental results show that the flow resistance measured from the miniature reed array correlates well with expected results based on the valve design geometry. To improve pump performance with the mini-reeds, the flow could be enhanced by redesigning the pump head with room for a larger valve array. Further testing

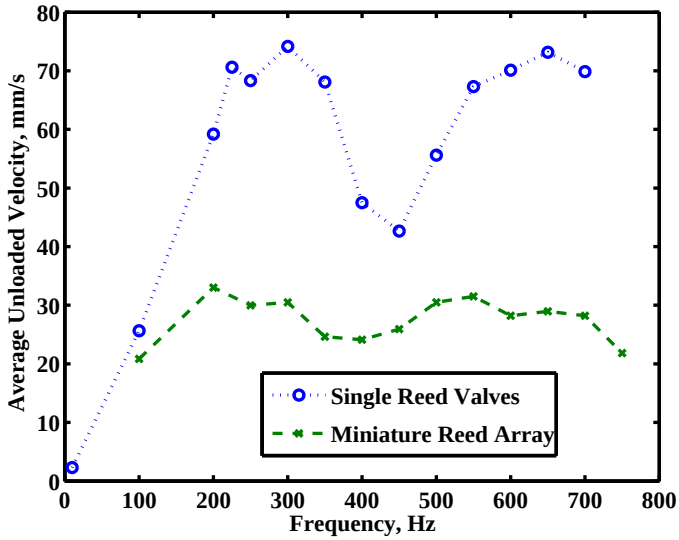

Figure 12. Unloaded test results for pump performance comparing the miniature reed array to the single-reed valves.

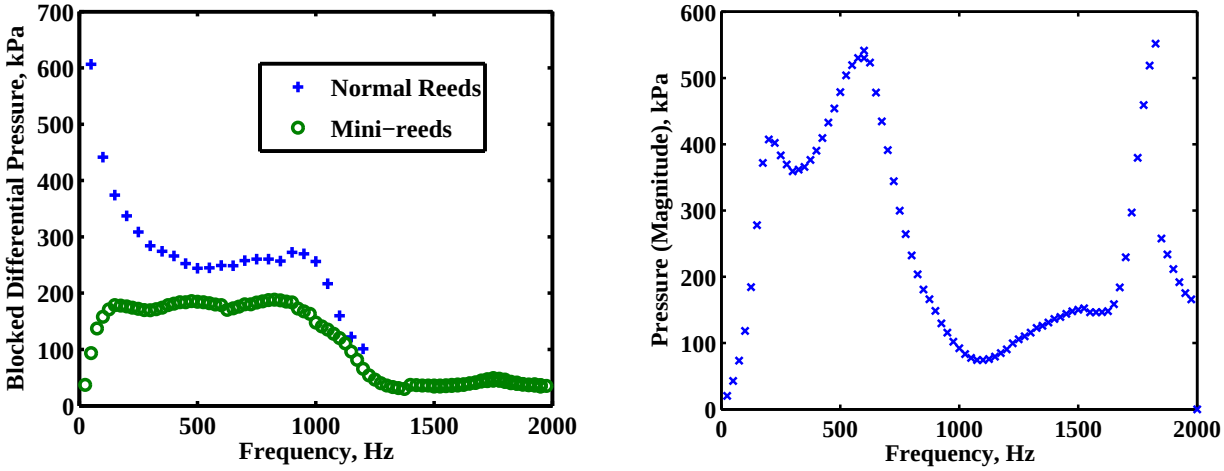

Figure 13. Blocked pressure results from a low current (1.4 A_{rms}) sinusoidal frequency sweep of the pump input comparing both types of valves (left). The same test was preformed with no valves installed, measuring the magnitude of the pressure wave generated (right).

demonstrated that the frequency bandwidth of the valve response may have been limited by the manifold and pump used for testing.

A 3-D fluid-structure interaction finite element model of a single-reed valve has been established and the results verified using in-situ measurements of the reed displacement. This model will now be used as a tool to evaluate future valve designs to enhance electro-hydrostatic actuator performance. The dynamic behavior of the single-reed valves was characterized, and compared to analytic predictions. The displacement dependent flow resistance and reed valve dynamic response were then represented with simplified equations which can be used to improve overall system models to better understand and improve actuator performance.

APPENDIX A. ADDED MASS OF VIBRATING PLATE

The effect on the first natural frequency of submerging a vibrating plate in fluid can be calculated by adding an added mass term, A_p, equal to the mass of fluid enclosed by rotating the plate about its longer axis; hence,

$$A_p = \rho l w^2, \tag{2}$$

where ρ is the density of the fluid, l and w are the length and width of the plate.[11] The decreased first natural frequency in the fluid, f_{fluid}, compared to the natural frequency in vacuum, f_{vacuum}, is then

$$\frac{f_{\text{fluid}}}{f_{\text{vacuum}}} = \left(1 + \frac{A_p}{M_p}\right)^{-1/2}, \tag{3}$$

where M_p is the mass of the plate.

ACKNOWLEDGMENTS

Financial support for this research was provided by the Smart Vehicle Concepts Center, a National Science Foundation Industry/University Collaborative Research Center (www.SmartVehicleCenter.org), and by the Ohio State University through a Smart Vehicle Concepts Graduate Fellowship. Technical advice was provided by Tom Greetham and Tom Walters of Moog, Inc. in East Aurora, NY. This work was supported in part by an allocation of computing time from the Ohio Supercomputer Center.

REFERENCES

[1] Lee, D., Shin, D., and Carman, G., "Large flow rate/high frequency microvalve array for high performance actuators," *Sensors and Actuators A: Physical* **134**(1), 257–263 (2007).

[2] Li, B. and Chen, Q., "Design and fabrication of in situ UV-LIGA assembled robust nickel micro check valves for compact hydraulic actuators," *Journal of Micromechanics and Microengineering* **15**, 1864 (2005).

[3] O'Neill, C. and Burchfield, J., "Kinetic Ceramics Piezoelectric Hydraulic Pumps," *Proc. SPIE* **6527**, 65270I (2007).

[4] Seong, M., Mohanchandra, K., Lin, Y., and Carman, G., "Development of a 'bi-layer lift-off' method for high flow rate and high frequency Nitinol MEMS valve fabrication," *Journal of Micromechanics and Microengineering* **18**, 075034 (2008).

[5] Eggeler, G., Hornbogen, E., Yawny, A., Heckmann, A., and Wagner, M., "Structural and functional fatigue of NiTi shape memory alloys," *Materials Science and Engineering A* **378**(1-2), 24–33 (2004).

[6] Chaudhuri, A., Yoo, J., and Wereley, N., "Design, test and model of a hybrid magnetostrictive hydraulic actuator," *Smart Materials and Structures* **18**, 085019 (2009).

[7] Walters, T., *Development Of A Smart Material Electrohydrostatic Actuator Considering Rectification Valve Dynamics And In Situ Valve Characterization*, Master's thesis, The Ohio State University (2008).

[8] Keller, C. A., *Novel Concepts in Piezohydraulic Pump Design*, Master's thesis, Georgia Institute of Technology (2004).

[9] Hamrock, B., Jacobson, B., and Schmid, S., [*Fundamentals of machine elements*], WCB/McGraw-Hill New York, USA (1999).

[10] Rupinsky, M. J., *Smart Material Electrohydrostatic Actuator for Intelligent Transportation Systems*, Master's thesis, The Ohio State University (2006).

[11] Blevins, R. D., [*Formulas for Natural Frequency and Mode Shape*], Van Nostrand Reinhold Company (1979).

[12] Herr, F., Mallin, T., Lane, J., and Roth, S., "A shock absorber model using CFD analysis and Easy5," SAE Technical Paper Series 1999-01-1322, SAE International (1999).

[13] Rupinsky, M. J. and Dapino, M. J., "Smart material electrohydrostatic actuator for intelligent transportation systems," *ASME Conference Proceedings* **2006**(47683), 721–730 (2006).